

2

AD-A258 030

1991



DTIC  
ELECTE  
NOV 30 1992  
S C D

Final Report for ONR Contract N00014-89-J-1573

MIXING AND FINESTRUCTURE PROCESSES IN A COASTAL JET  
DURING OPTOMA-21

Principal Investigator: Libe Washburn

Department of Geography  
University of California  
Santa Barbara, CA 93106-4030

Phone: (805)-893-7045  
Telemail: L.WASHBURN (OMNET)

DISTRIBUTION STATEMENT A  
Approved for public release  
Distribution Unlimited

92 11 30 016

92-30374



~~01916 102~~

2308

## 1. SUMMARY

High resolution tow-yo observations obtained during the OPTOMA21 cruise are used to examine finestructure and microstructure processes in a strong coastal jet which was observed off the coast of Northern California in July, 1986. Results from a combined CTD and XBT survey reveal that the jet is baroclinic and has a geostrophic velocity field extending to at least 500 m. The jet has a horizontal scale of about 40 km and is readily identified in SST imagery because it entrains cold upwelled water from the coastal region and advects it far off shore. The width of the thermal signature at the surface is 15 - 20 km, much smaller than the width of the velocity signature. Analysis of Reinecker and Mooers (1989) found that the jet is embedded in a large scale eddy field and is located between a pair of eddies, one cyclonic and the other anti-cyclonic.

Anomalies in temperature and salinity are commonly found in the upper 120 m of the water column and are the result of thermohaline intrusions. The intrusions are typically found on the cyclonic side of the coastal jet, and have anomalously high temperature and salinity compared to surrounding filament waters. These intrusions are oriented parallel to the local density field and have aspect ratios as great as 1500 to 1. Conductivity microstructure data are available for some of the sections and these show that the intrusions are often associated with high mixing rates. Mixing layers occur on the upper and lower boundaries of one particularly strong intrusion and are horizontally coherent for about 15 km. The properties of the intrusion suggest that it originated from low velocity waters to the south of the filament. While density ratios in the boundaries of the intrusion are low (about 1.3), Cox numbers in the events are too large (order 1000) to be accounted for by diffusive processes. Small scale intrusions are also found within other frontal regions on the boundaries of the jet. Other regions of strong mixing activity are observed at the base of the surface layer and are likely the result of wind induced turbulence in the mixed layer.

Evidence for subduction processes, which may be partly responsible for formation of the intrusion, is found in both the offshore and inshore regions of the filament. High levels of chlorophyll fluorescence at depths exceeding 100 m are found inshore and suggest rapid sinking of these waters. Offshore, a sub-surface intrusion is found in association with a density compensated frontal region.

DTIC QUALITY INSPECTED 2

## 2. INTRODUCTION

A major focus of this analysis is the various physical processes leading to water mass conversion in the offshore flowing jets commonly observed in the coastal transition zone. Evidence for this conversion comes from an observed systematic change in water properties out the jet axis which suggests that lateral or isopycnal mixing and advective processes are active in regions of high vorticity on the jet boundaries. The primary observations are temperature T, salinity S, and potential density  $\sigma_\theta$  down to scales of about 1 m along with current shear measured with an acoustic velocity profiler Doppler (ADCP). From an observational point of view, the isopycnal mixing processes produce signatures consisting of T-S finestructure in the form of local minima and maxima. A new feature of this study compared with others is that we have fairly high horizontal resolution so water masses on horizontal scales of about 1 km may be detected. An observational goal of this study is to look for these small scale water masses and

Accession No.	
NTIS	
DTIC TAB	
Unannounced	
Justification	
Per Hts.	
Distribution/	
Availability	
Avail and	
Dist	Special

A-1

try to answer questions such as:

- a) What are the isopycnal and diapycnal scales of thermohaline intrusions in the jet?
- b) Are these intrusions important in transforming the water mass structure of the jet?
- c) What is the orientation of the intrusions to the local density structure?
- d) Can the "parent" water masses from which the intrusions are derived be identified?
- e) Are the intrusions found mainly in regions of high vorticity or do they occur randomly with respect to the jet? Do they occur outside the jet?
- f) Is increased small scale turbulence associated with the intrusions and, if so, what processes are responsible for producing the turbulence? This is an important question because the observation of small scale turbulence in the intrusions would indicate a link between lateral mixing and stirring processes and turbulent diapycnal transport.

### 3. INSTRUMENTATION AND OBSERVATIONS

The instrumentation deployed during OPTOMA21 consisted of a standard CTD/rosette package used to do the hydrographic survey and a tow-yo platform which carried a Neil Brown CTD, a conductivity microstructure instrument, a fluorometer, a transmissometer and an electromagnetic current meter. The conductivity sensor has a spatial resolution of about 1 cm and is adequate for resolving turbulence generated temperature fluctuations in the filament; a more complete description of the system and sensor characteristics is given by Washburn and Deaton (1986). For our analysis the microconductivity signal is assumed to be mainly a function of temperature and is used to estimate the temperature variance dissipation rate  $\chi_T$  (hereafter indicated as  $\chi$ ) and the Cox number  $C$  (cf. Osborn and Cox, 1972; Gargett, 1984; Dillon, 1982; Washburn, 1987).

The instrument platform itself is constructed from a long section of aluminum channel with a fin extending rearward to maintain the orientation of the sensors into the flow. Normally this platform was deployed as the research vessel moved down swell; this greatly decreased the effects of ship motion on the platform compared with towing into the swell. The high resolution sections were obtained during tow-yo profiling in which the instrumented platform was profiled (by winching) between the surface and about 120 m as the research vessel was underway at about 4 knots (~ 2 m/s).

During the CTD and tow-yo sections, XBT's were also deployed to resolve the deep geostrophic flow field. The complete pattern of CTD and XBT stations are shown by Reinecker and Mooers, (1989). Beginning with tow-yo section T3 (described below), acoustic Doppler velocity data is also available for computing vertical shear of horizontal currents and absolute current velocities where good navigation data is available.

#### 4. THERMOHALINE STRUCTURE

During the OPTOMA21 cruise from 7-20 July 1986, two upwelling filament systems were apparent in the area between Pt. Arena and Pt. Reyes as may be seen in the satellite SST image of Fig. 1 taken on 16 July 1986. These filaments are recurrent features of the area (eg. Huyer and Kosro, 1987 and Kosro, 1987). Cool water appears white in the image and two distinct filaments are evident, one extending offshore from Pt. Arena and a second offshore from Pt. Reyes. This latter filament off Pt. Arena was the object of the OPTOMA21 field experiment. An upwelling center from which some of the cold surface water of the system is apparently derived lies between Pt. Reyes and Pt. Arena.

The analysis of this report focuses on results from two tracks from the OPTOMA21 experiment are shown in Fig. 1 labelled T 2 and T3. High quality microstructure data and ADCP data were obtained along T3; instrument problems prevented acquisition of these data on T2, although CTD data were obtained. As will be shown, observations along track 2 which crosses track 3 show thermohaline structure very consistent with that along track 3. An interesting feature of both T2 and T3 is that they cross the cold filament in two places and effectively allow sampling at two points along the filament axis. The interactions of the filament with the surrounding water masses results in evolution of water mass characteristics within the filament between the two crossing points of these tow tracks.

The regions of cool water (light shading in Fig. 1) crossed by T2 and T3 also correspond to regions of strong geostrophic flow, referenced to 750 dbar, as shown by Reinecker and Mooers (1989), although the horizontal, cross axis scale of the jet is about 40 km while the width of the cool filament at the surface is only about 15 to 20 km (Fig. 2). Jones et al (1991) have shown that SST contours obtained from the in situ measurements agree with the SST imagery of Figure 1 in that an extensive cool filament consisting of coastally upwelled surface water is found in situ. The offshore volume transport in the jet is of order 2 Sv ( $1 \text{ Sv} = 10^6 \text{ m}^3/\text{s}$ ) and is comparable to other filament observations (eg. Kosro, 1987; Washburn and Armi, 1988). An interesting feature of the section is that a comparably strong onshore flow is evident at the southern end of the section and corresponds to the part of the filament mentioned above which bends back toward shore (Reinecker and Mooers, 1989). This change in direction of the jet suggests that the filament may be part of a meandering coastal current system such as those discussed by Strub et al. (1991).

From the T3 temperature section of Fig. 2 it may be seen that minimum surface temperatures in the cool filament are about 12.75 C. The time of T3 was one day after the image of Fig. 1, but a strong correspondence is observed between the in situ data and the satellite image so the flow field did not evolve substantially over this period. Detailed examination of near surface tow-yo temperature and salinity profiles in the region where T3 intersects this onshore flow suggest that more saline water from south of the filament is being subducted under filament waters. Subduction within near shore and offshore regions of coastal jets have been reported recently by Washburn, et al. (1991), Kadko, et al (1991), and Jones et al. (1991). Subduction processes are likely to be a very important secondary flow mechanism in coastal jets since they result in vertical transport of water properties, nutrients, and other scalars, along with phytoplankton. These processes act in well stratified waters (with little small scale

turbulent transport) and have vertical velocities as large as 30 m/day; they may be a dominant process in these coastal upwelling systems.

The surface temperature front at the filament boundary along T3 also corresponds to a density front because horizontal salinity differences were relatively small and the maximum horizontal salinity gradient does not coincide with the maximum horizontal temperature gradient (Fig. 2B). Horizontal density changes across the temperature front at 36 km in T3 are about  $0.5 \text{ kg/m}^3$  (Fig. 2C). The region of these high temperature and density gradients is located at the center of the geostrophic jet reported by Reinecker and Mooers (1989) and may result from strong near surface convergence along the jet axis. Convergence regions have been observed from drifter data in a strong coastal jet which was present in this area during the Coastal Transition Zone Experiment in 1988 (Swenson, et al. 1991).

The second crossing of the filament and jet axis is identifiable in the temperature section from T3 by a region of cool water between 105 and 130 km, although near surface temperatures are somewhat warmer compared with the first crossing in T3. Near surface salinity and density are lower than the first crossing and these variations in water properties are consistent with lateral mixing between water masses near the jet axis and those lying outside the jet. The time scale for this mixing to occur is may be estimated from the advection time out and around the jet axis and is of order a few days.

Sections comparable to those of T3 were obtained two days earlier along T2 (see Fig. 1 for tow track) and in general show much the same overall structure. This is interesting because it means that significant evolution of the subsurface T-S structure did not occur on this time scale. Somewhat better resolution of the return flow portion of the jet and filament system was obtained during T2 as may be seen in Fig. 3A where a distinct, isolated region of cool water is observed between 75 and 95 km in the upper 40 m of the water column. It is surrounded by warmer waters on either side and is also in a region of onshore flow (Reinecker and Mooers, 1989). The geostrophic signature of the jet is evident in the density contours of both T3 and T2: for example: over the first 70 km of T2, isopycnal surfaces below the mixed layer slope upwards along the track. This may be clearly seen for the 25.80 surface which is about 117 m at the beginning of the section, but rises to about 47 m depth at 63 km along the track. Other surfaces have comparable slopes in this part of the tow track and are consistent with offshore geostrophic flow to depths exceeding 120 m. Beyond 70 km isopycnal surfaces deepen rapidly in the region of onshore flow where the jet has bent back toward shore.

## 5. FRONTAL FINESTRUCTURE

One mechanism which could result in the change in water mass properties between the offshore flowing and onshore flowing portions of the jet is suggested through careful examination of the salinity section of T3, namely, the occurrence of thermohaline intrusions. Between 35 and 55 km in the depth range 55 to 85 m an isolated region of high salinity is found and it is evident in the salinity section as a region of closed contours. The anomaly, or intrusion, here is about 0.15 psu above the surrounding waters and appears to be strongly tilted in the cross jet direction. The region is statically stable since density increases continuously through the feature (Fig. 2C) and it has a much weaker signature in the temperature contours with no region of isolated contours at this contour interval (Fig. 2A).

An expanded view of the salinity anomaly confirms that it is very thin, only about 10 m, and has a horizontal extent of about 15 km (Fig. 4A); thus the aspect ratio is about 1500 to 1. Since this is only a single cross section through the feature it may be extensive in the along-axis direction of the jet. A superposition of high salinity regions ( $S > 33.30$  psu) and density contours clearly shows that the tilt of the intrusion is identical to the local slope of isopycnal surfaces (Fig. 4B) and that the range of isopycnals containing the intrusion is in the range 25.30 to 25.60. A possible source water mass for this intrusion is also suggested in Fig. 4B where  $S > 33.30$  psu is found in the same density range as in the intrusion beginning at 65 km or about 10 km from the intrusion. This is part of a larger water mass (Fig. 2B) which is found on the cyclonic side of the coastal jet.

Similar evidence of intrusive activity is also found in the frontal region of the jet farther along T2 where the jet bends toward shore. Numerous, isolated regions of salinity maxima and minima mark thermohaline intrusions (Fig. 5A) and superposition of high salinity regions ( $S > 32.95$  psu) on the density field show that they tilt with the local density field (Fig. 5B). The water column is thermally stratified in both of these frontal regions so salinity is a good tracer for intrusive activity here. Intrusive activity in section T2 was much less apparent than in T3 and may reflect high spatial variability of intrusions in this system.

## 6. SMALL SCALE MIXING ACTIVITY IN JET

An interesting feature of at least some of the intrusions on the cyclonic side of the jet is the occurrence of small scale mixing activity on their upper and lower boundaries. A clear example of this is shown in Fig. 6 in the right hand panel where high levels of  $\chi$ , the temperature variance dissipation rate, are observed on the upper and lower boundaries of the deep salinity maximum centered at 80 m which marks the intrusion. This is the same intrusion shown in Figures 4A and 4B and the position of this particular profile (number 717) is indicated by an arrow at the top of Fig. 4A. Only portions of the  $\chi$  profile which exceed the instrumental noise level ( $\chi_{\text{noise}} \sim 10^{-8} \text{ C}^2/\text{s}$ ) are shown. Note that the apparent noise level of the system seems to change with time; this is an artifact due to the constantly changing speed of the instrument platform through the water. For comparison the high frequency contribution to the conductivity variance is also shown and is seen to be roughly proportional to  $\chi$  when both are above the noise level. The dynamic range of the conductivity variance  $V$  is greater because it is dominated by higher spectral levels at lower frequencies where spectral noise levels are smaller.

Mixing rates are high in two parts of the  $\chi$  profile of Fig. 6. Near the surface mixing activity is probably wind driven and extends vertically through the water column to about 40 m. The highest levels in the entire profile,  $\chi > 10^{-5} \text{ C}^2/\text{s}$  are found on the lower boundary of the intrusion and occupy a mixing layer about 10 m thick. A second, thinner and weaker mixing region is observed on the upper boundary of the same intrusion. Another layer of strong mixing activity in a region which is diffusively stable occurs between 95 and 110 m.

A set of profiles more typical of average conditions in the California Current System is shown in Fig. 7 (profile 648) and its position is identified by the arrow along the upper boundary of Fig. 2B. This profile is well outside of the jet and shows a deep mixed layer to about 40 m

with a local maximum in buoyancy frequency  $N$ . The  $N$  profile within the jet at station 717 is much more complex with multiple maxima throughout the water column. Mixing activity is also more concentrated near the surface outside the jet with maximum  $\chi$  levels occurring at the base of the mixed layer. Low levels of  $\chi$  near the surface are due to decreasing mean vertical temperature gradients.

The Cox numbers associated with these layers are of order 1000 and are consistent with fairly strong turbulent transport of salt out of the intrusion; this distribution of mixing activity would tend to decrease the salinity of the intrusion and might be one factor in governing its evolution. A lower bound for the timescale for destruction of the intrusion by small scale turbulence may be estimated from these observations of mixing activity. First, assume that the intrusion is uniform and is 10 m thick (ie. Fig. 4A) and that the average Cox number  $C$  in the vicinity of the intrusion is of order 500. Using a simple one-dimensional model of salt diffusion where the initial salinity anomaly is a "top hat distribution", the salinity anomaly will evolve according to,

$$S(z=0,t)/S(0,0) = \text{erf}\{z_0/[2(K_z t)]^{1/2}\}$$

where erf is the error function,  $K_z$  is the eddy diffusivity, and  $z_0$  is the initial half thickness of the intrusion. The time  $t$  required to reduce the center line salinity by a factor of  $1/e$  is therefore specified by,

$$\text{erf}\{z_0/[2(K_z t)]^{1/2}\} = e^{-1}$$

With  $K_z = 0.7 \times 10^{-4} \text{ m}^2/\text{s}$  (corresponding to  $C = 500$ ), the time scale is about 9 days. For comparison the same timescale using the molecular diffusivity for salt in place of  $K_z$  is about  $10^3$  years. Given advection speeds in the jet at the depth of the intrusion of 0.3 m/s, the intrusion may have originated as much as 300 km "upstream" in the jet.

Double diffusion (salt fingering) is one process which might account for the observed mixing layers on the lower boundary of the intrusion although two factors seem to argue against this mechanism. First, the observed Cox number levels of 500 to 1000 seem too high. Microstructure observations in other systems where salt fingering is clearly dominant such as the C-SALT region in the Caribbean show that Cox numbers are generally in the range 10 - 20 (cf. Marmorino, 1989). Second, no organized staircase structures are observed under any of the intrusions as is commonly observed in salt fingering-dominated systems.

## 7. DISCUSSION AND CONCLUSIONS

High resolution towed CTD/microstructure observations were obtained as part of the OPTOMA21 cruise in July 1986. These have been combined with a large scale CTD/XBT survey to construct a detailed picture of the thermohaline structure of a strong baroclinic jet which was present off Northern California in the vicinity of Pt. Reys and Pt. Arena.

Extensive finestructure in temperature and salinity fields revealed the presence of thermohaline intrusions in the jet, although the signatures are most apparent in the salinity field. Where small scale mixing measurements were available, high levels of the temperature

dissipation rate  $\chi$  were observed on the boundaries of the intrusions. The intrusions appear to be much more common in the coastal jet than in the surrounding water masses.

Because these tow-yo sections consist of over 200 profiles each, the cross jet axis extent of the intrusions can be determined to horizontal scales of about 1 km and their orientation with respect to the local density field determined. It is found that even at the smallest resolved horizontal scales, the intrusions lie along isopycnal surfaces. Furthermore, the properties within the intrusions are consistent with formation from parent water masses which lie at the same density levels. We hypothesize that the intrusions result from lateral instabilities of some type and advect and mix along isopycnal surfaces. The horizontal extent of the instability processes are not known, but may be at least 10 km based on observed property distributions. Instabilities on these scales have been observed in the mixed layer on a similar coastal jet by Washburn and Armi (1988).

Because of the strong geostrophic flow of the jet, isopycnal surfaces slope sharply in the cross jet direction so isopycnal advection will also lead to rapid vertical movement of the intrusions. The observed levels of mixing rate suggest that the intrusions may not be locally formed since their decay time due to turbulent diffusion is of order several days. However processes other than small scale turbulence may be important in the evolution of the intrusions.

We speculate that the intrusions may form near shore and be advected offshore and downward away from their generation sites, although more observations at these horizontal scales are required to characterize their distributions. We also suggest that the observation of strong mixing activity on the intrusions indicates a link between diapycnal and isopycnal mixing processes in high vorticity regions of baroclinic jets. If this is true, then useful parameterizations of small scale, vertical eddy diffusivities may require larger scale, horizontal (or isopycnal) instability processes be taken into account.

## 8. REFERENCES

- Dillon, T.M., 1982. The energetics of over-turning structures: implications for the theory of fossil turbulence, *J. Phys. Oceanogr.*, 14, 541-545.
- Gargett, A.E., 1984. Vertical eddy diffusivity in the ocean interior, *J. Marine Res.*, 42, 359-353.
- Huyer, A., and P.M. Kosro, 1987. Mesoscale surveys over the shelf and slope in the upwelling region near Pt. Arena, *J. Geophys. Res.*, 92, C2, 1655-1681.
- Jones, B.H., C.N.K. Mooers, M.M. Reinecker, T.P. Stanton, and L. Washburn, 1991. Chemical and biological structure of a cool filament observed off Northern California in July 1991 (OPTOMA21), accepted for publication, *J. Geophys. Res.*
- Kadko, D.C., L. Washburn, and B.H. Jones, 1991. Evidence for subduction within cold filaments of the Northern California Coastal Transition Zone, *J. Geophys. Res.*, 96, C8, 14,909-14,926.

- Kosro, P.M., 1987. Structure of the coastal current field off Northern California during the Coastal Ocean Dynamics Experiment, *J. Geophys. Res.*, 92(C2), 1637-1654.
- Marmorino, G.O., 1989. Substructure of oceanic salt finger interfaces, *J. Geophys. Res.*, 94, C4, 4891-4904.
- Reinecker, M.M., and C.N.K. Mooers, 1989. Mesoscale eddies, jets, and fronts off Point Arena, California, July 1986, *J. Geophys. Res.*, 9, 12,555-12,570.
- Osborn, T.R., and C.S. Cox, 1972. Oceanic finestructure, *Geophys. Fluid Dynamics*, 3, 321-345.
- Strub, P.T., P.M. Kosro, A. Huyer, C. James, L.J. Walstad, R.L. Smith, J.A. Barth, R.R. Hood, M.R. Abbot, K.H. Brink, T.L. Hayward, P.P. Niiler, M.S. Swenson, R.K. Dewey, F. Chavez, S.R. Ramp, M.L. Batteen, R.L. Haney, D.L. Mackas, L. Washburn, D.C. Kadko, R.T. Barber, D.B. Haidvogel, 1991. The nature of cold filaments in the California Current System, *J. Geophys. Res.*, 96, C8, 14,743-14,768.
- Swenson, M., P.P. Niiler, and K. Brink, 1991. The dynamical and thermodynamical structure of the flow associated with a cold filament off Pt. Arena, California in July 1988, submitted to *J. Geophys. Res.*
- Washburn, L., 1987. Two-dimensional observations of temperature microstructure in a coastal region, *J. Geophys. Res.*, 92(C10), 10,787-10798.
- Washburn, L., D.C. Kadko, B.H. Jones, T. Hayward, P.M. Kosro, T.P. Stanton, S.Ramp, and T. Cowles, Water mass subduction and the transport of phytoplankton in a coastal upwelling system, *J. Geophys. Res.*, 96, C8, 14,927-14,945.
- Washburn, L. and L. Armi, 1988. Observations of frontal instabilities on an upwelling filament, in press, *J. Phys. Oceanogr.*
- Washburn, L., and T.K. Deaton, 1986. A simple system for mapping conductivity microstructure, *J. Atmospheric and Oceanic Tech.*, 3, 3, 345-355.

## 9. FIGURE CAPTIONS

Figure 1. Satellite sea surface temperature image from 16 July 1986. Tow-yo tracks T2 and T3 are identified. Light shading corresponds to cool water, dark shading to warm water.

Figure 2A. Vertical section of temperature along track T3. Stippling corresponds to temperatures greater than 13.5 C. Arrow along upper boundary shows location of profile 648 shown in Fig. 7.

Figure 2B. As in 2A, but for salinity. Stippling corresponds to salinities less than 32.7 psu and hatching to salinities greater than 33.20 psu.

Figure 2C. As in 2A, but for potential density. Hatching corresponds to potential density less than 24.70.

Figure 3A. As in 2A, but temperature along track T2.

Figure 3B. As in 2B, but salinity along track T2. Stippling corresponds to salinities less than 32.80 psu and hatching to salinities greater than 33.20 psu.

Figure 3C. As in 2A, but potential density along track T2.

Figure 4A. High resolution section of salinity along track T3. Stippling corresponds to salinities less than 32.80 psu and hatching to salinities greater than 33.20 psu. Arrow along upper boundary of section shows location of profile 717 shown in Figure 6.

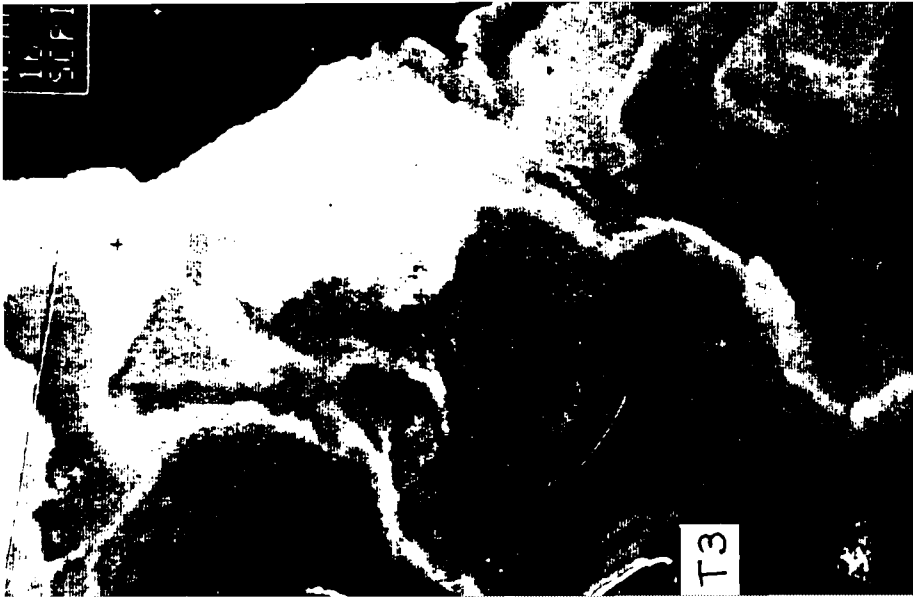
Figure 4B. High resolution section of potential density along track T3. Hatching corresponds to regions where salinity exceeds 33.20 psu.

Figure 5A. High resolution section of salinity along track T3 through return flow of jet. Stippling corresponds to salinities less than 32.80 psu and hatching to salinities greater than 32.95 psu.

Figure 5B. High resolution section of potential density along track T3 through return flow of jet. Hatching corresponds to regions where salinity exceeds 32.95 psu.

Figure 6. Vertical profiles of salinity, temperature, potential density, buoyancy frequency, temperature variance dissipation rate  $\chi$  (bold line) and conductivity variance (thin line) for profile 717. Location of this profile shown by arrow at top of Fig. 4A.

Figure 7. Vertical profiles of salinity, temperature, potential density, buoyancy frequency, temperature variance dissipation rate  $\chi$  (bold line) and conductivity variance (thin line) for profile 717. Location of this profile shown by arrow at top of Fig. 2A.



TEMPERATURE DEG (C) OPT 21 TRANSECT 3

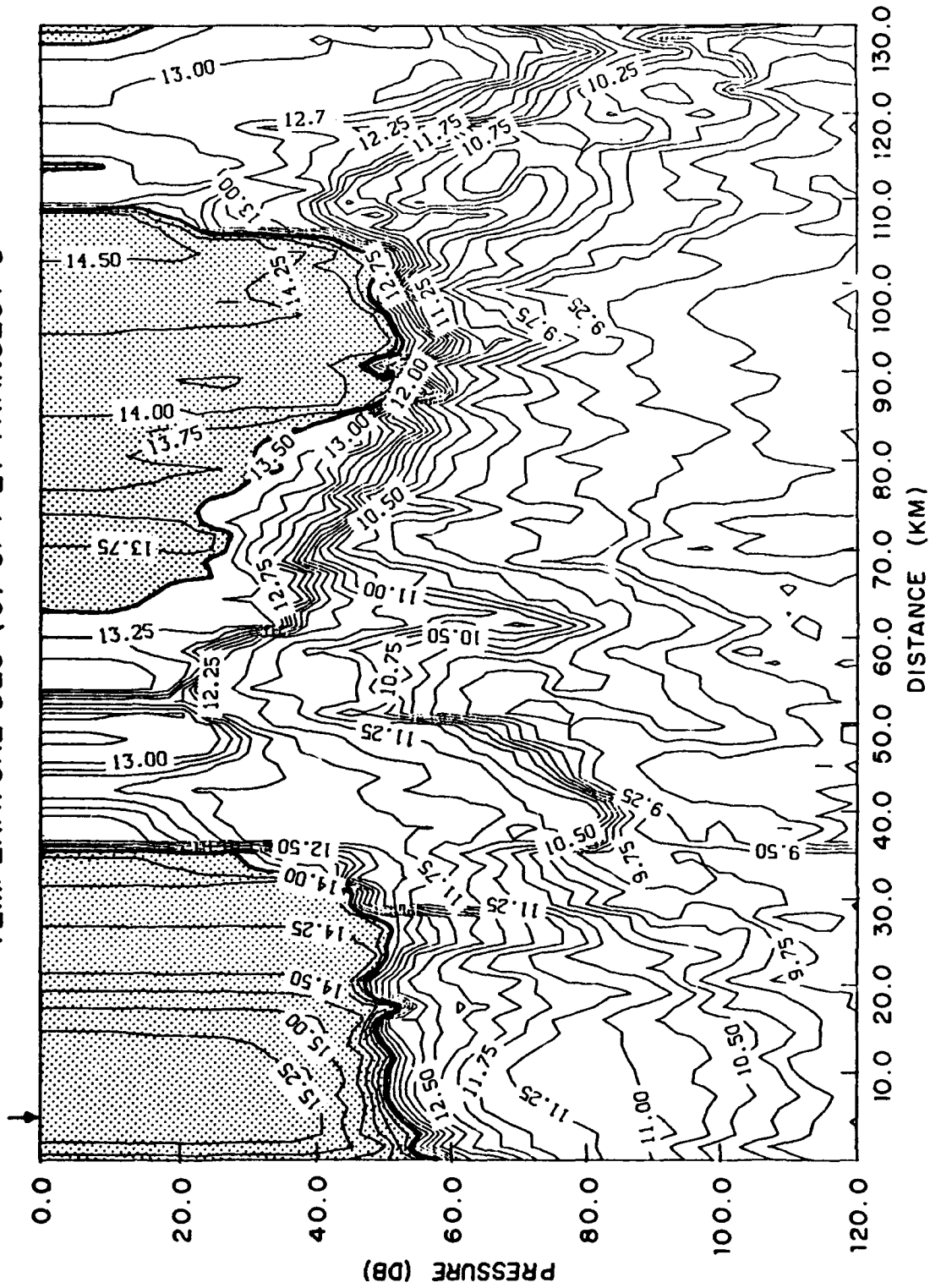


FIG. 2A

SALINITY (psu) OPT 21 TRANSECT 3

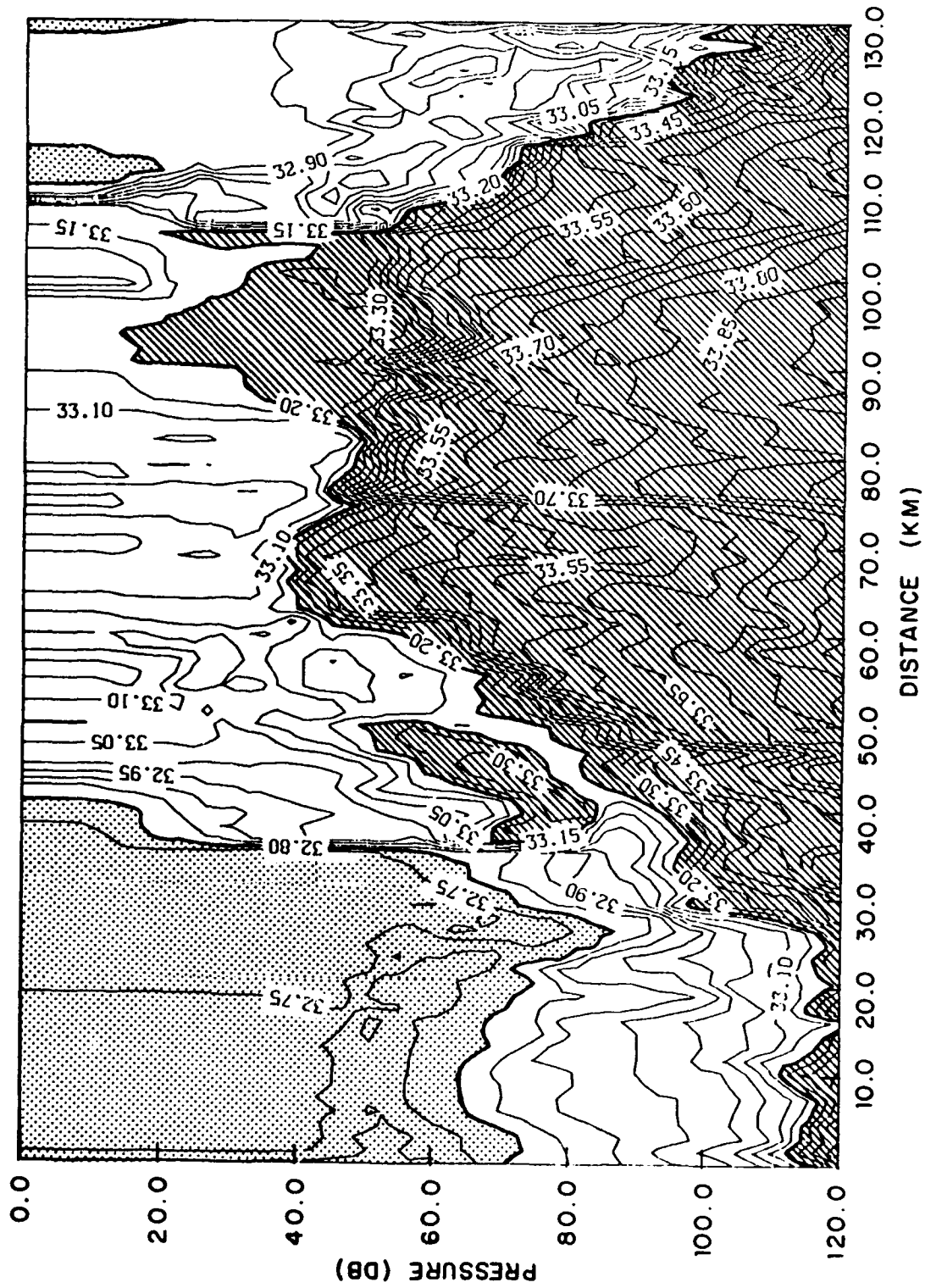


FIG. 2B

SIGMA THETA ( $\text{Kg}/\text{m}^3$ ) OPT 21 TRANSECT 3

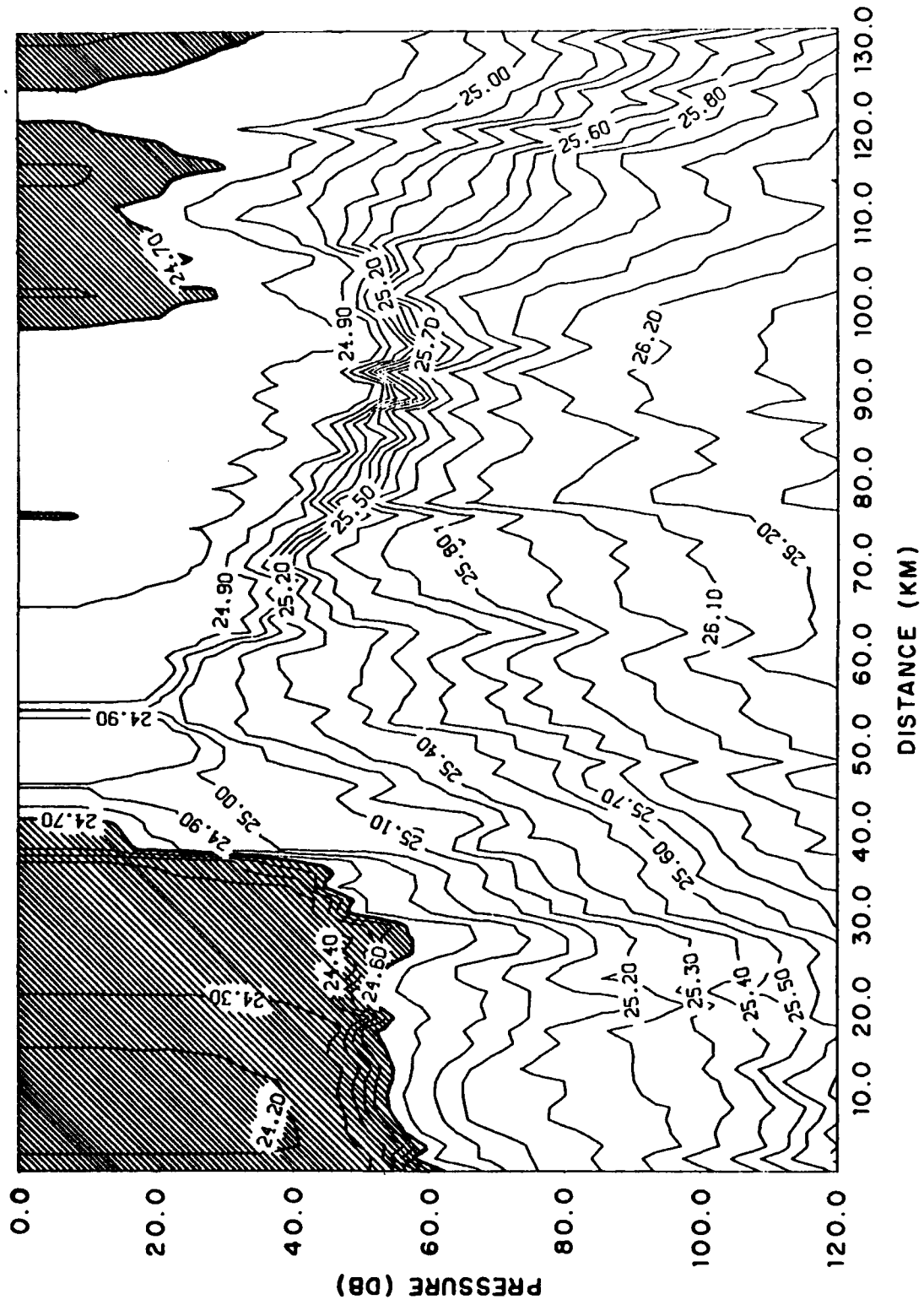


FIG. 2 C

OPT21 TRANSECT 2

TEMPERATURE DEG (C)

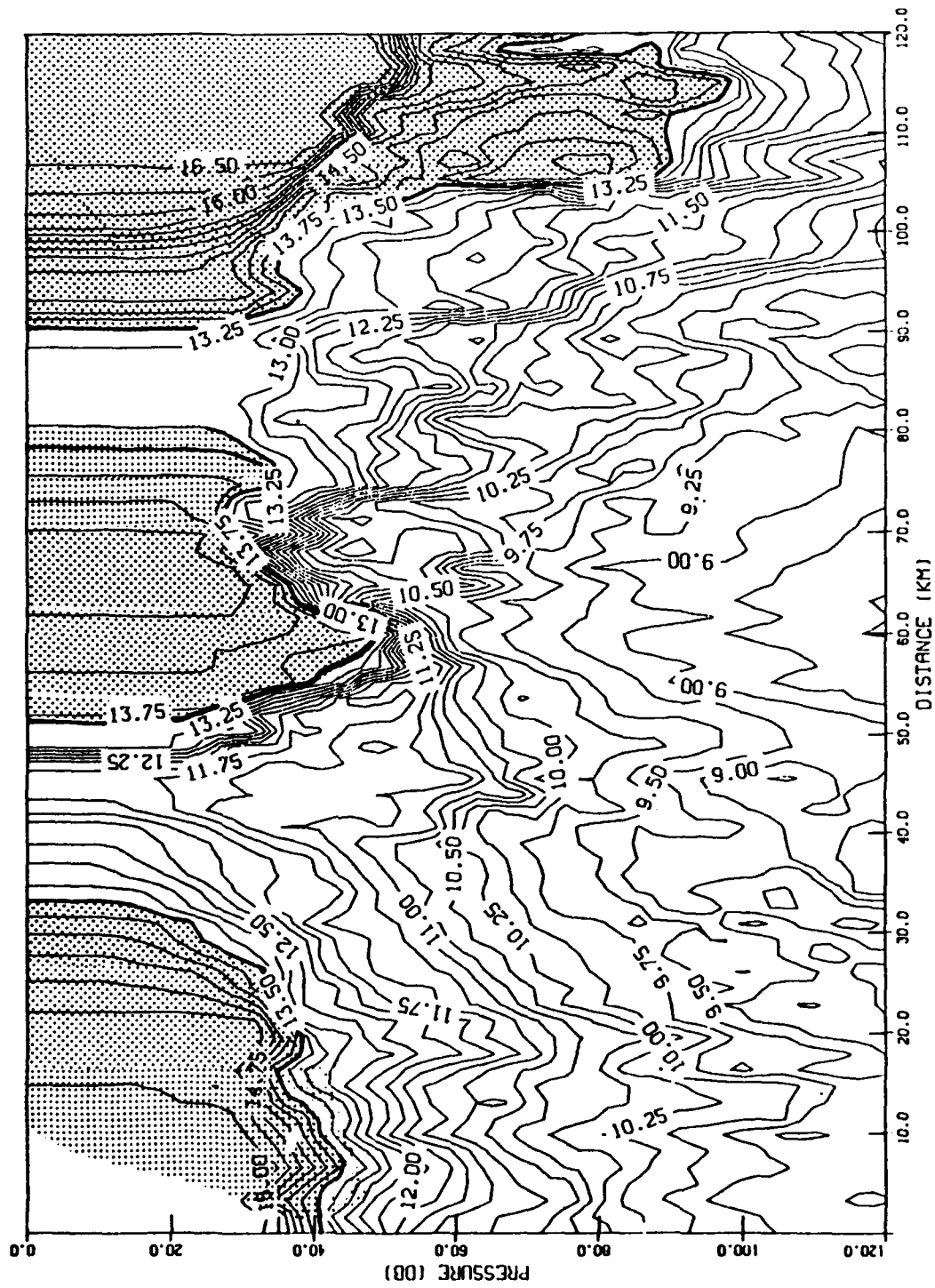


FIG. 3A

SALINITY (psu) OPT 21 TRANSECT 2

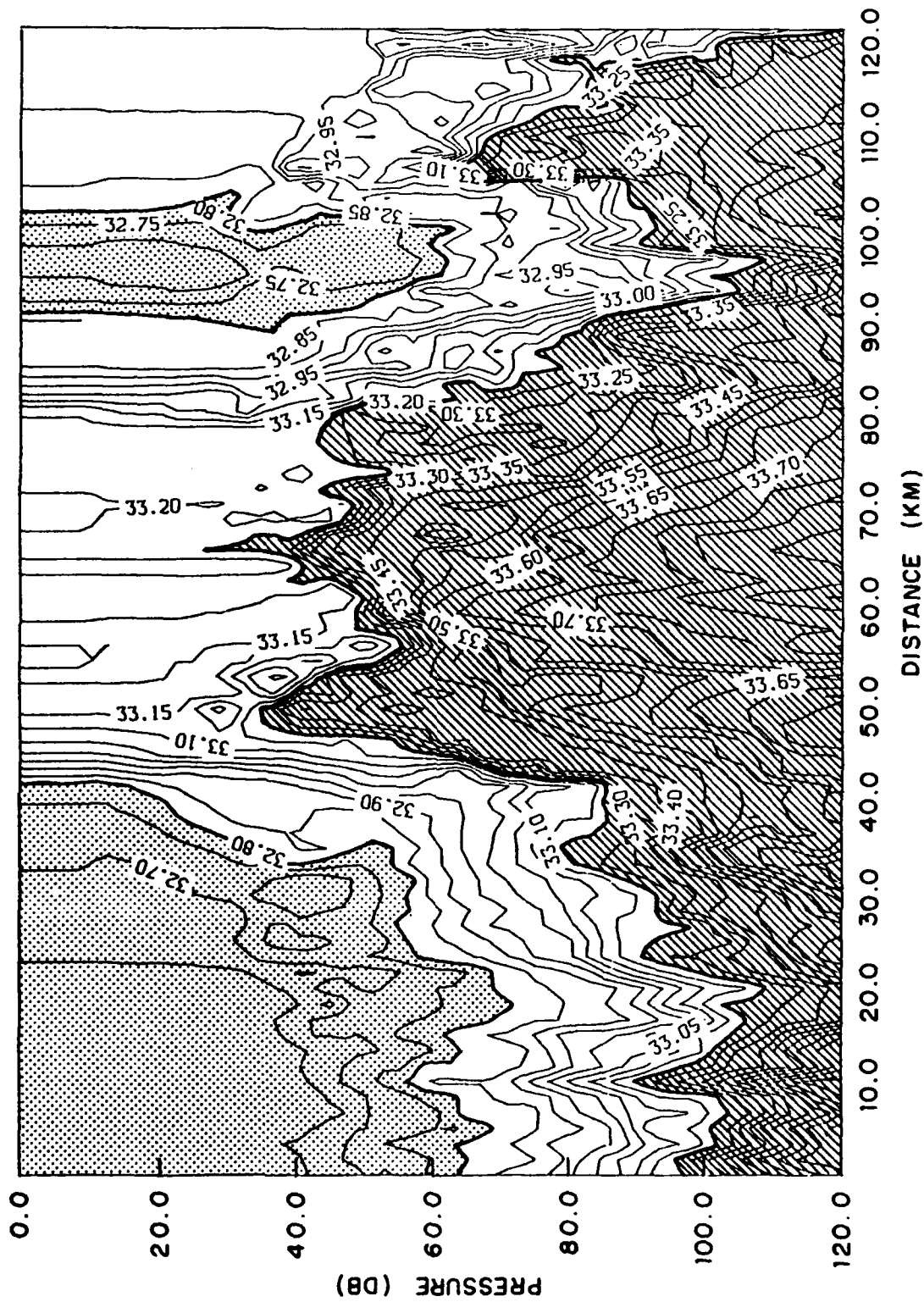


Fig. 3B

SIGMA THETA ( $\text{Kg/m}^3$ ) OPT 21 TRANSECT 2

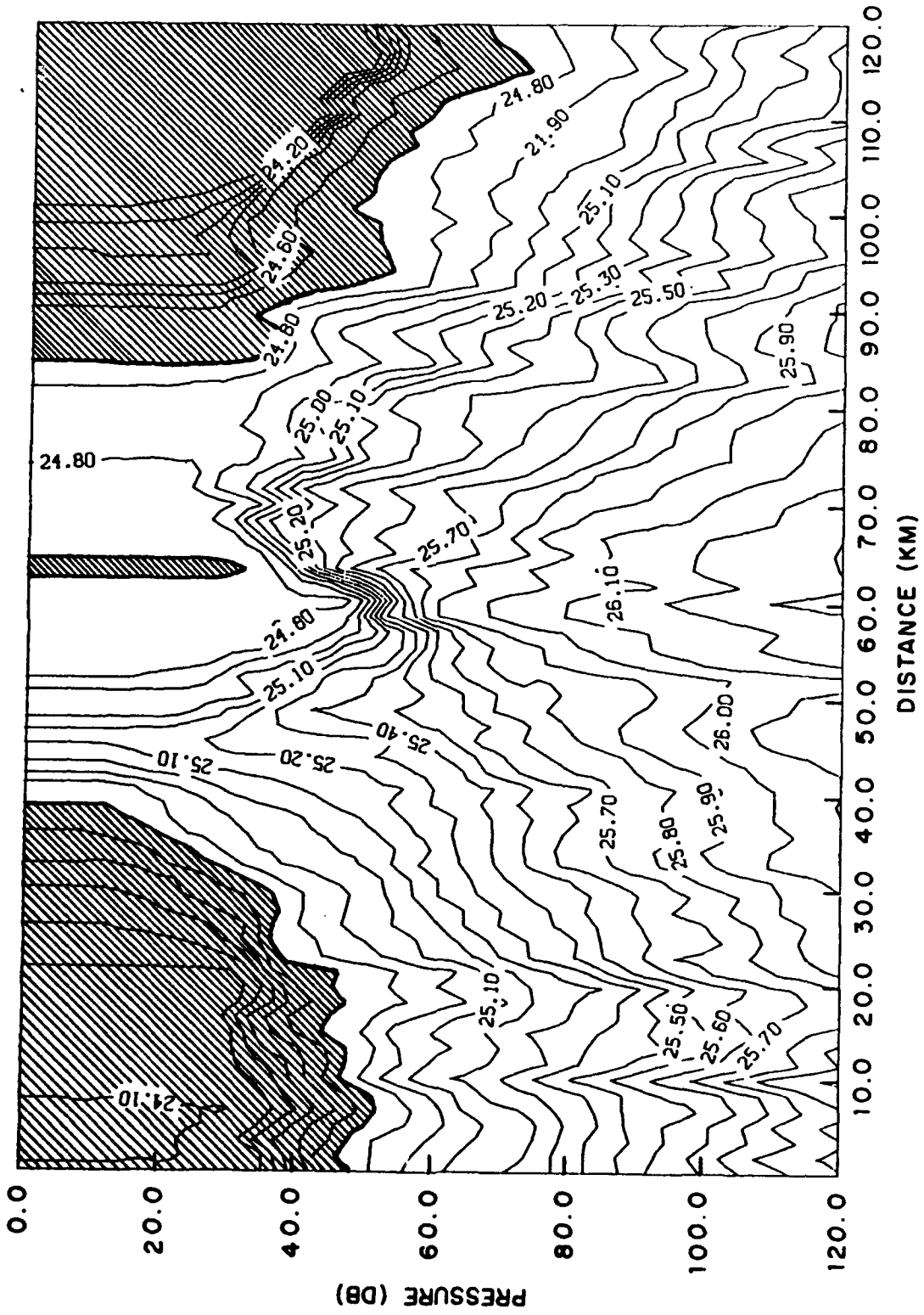


Fig. 3C

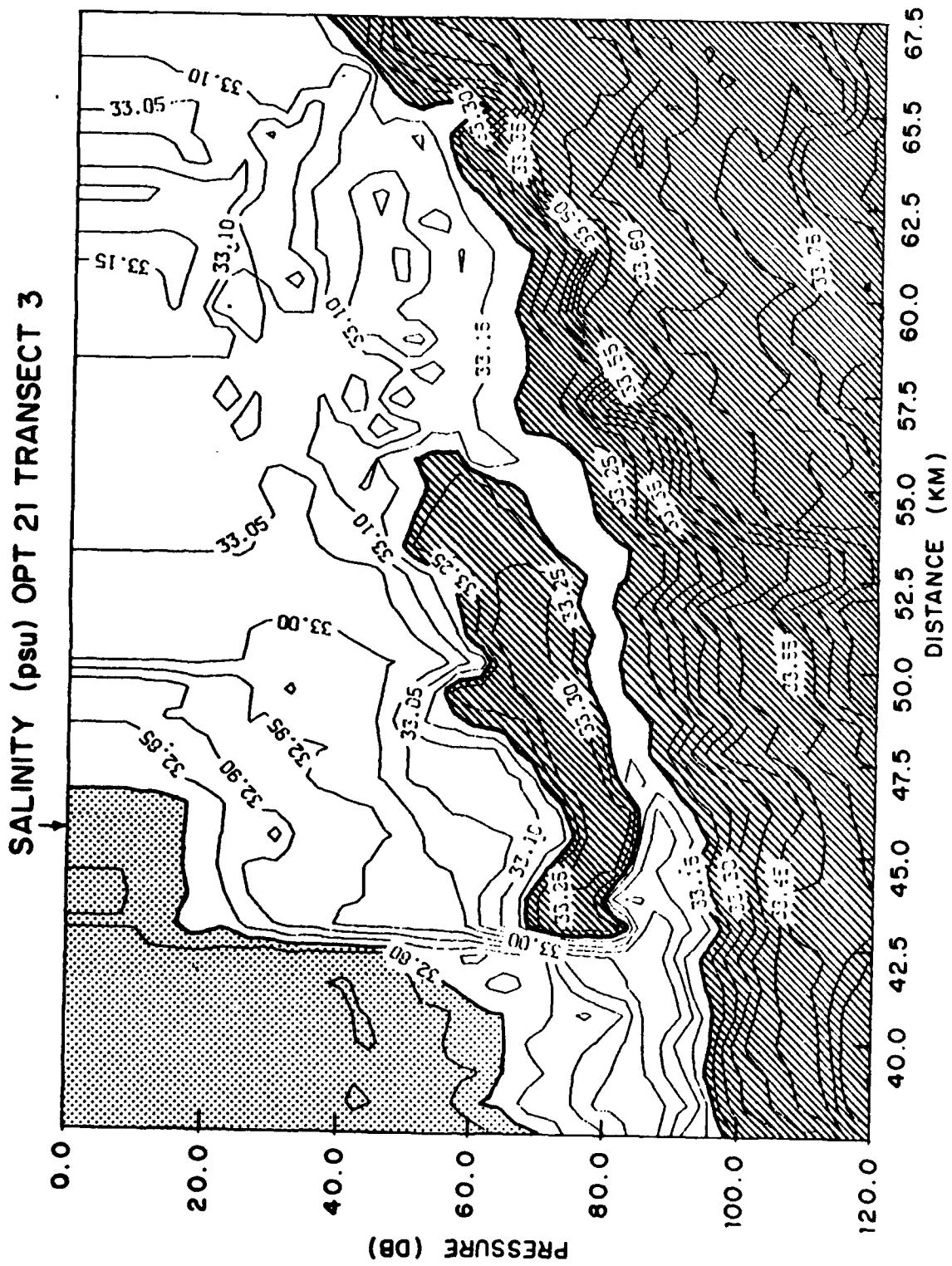


FIG. 4A

$\sigma_0$  (Kg/m<sup>3</sup>) OPT 21 TRANSECT 3

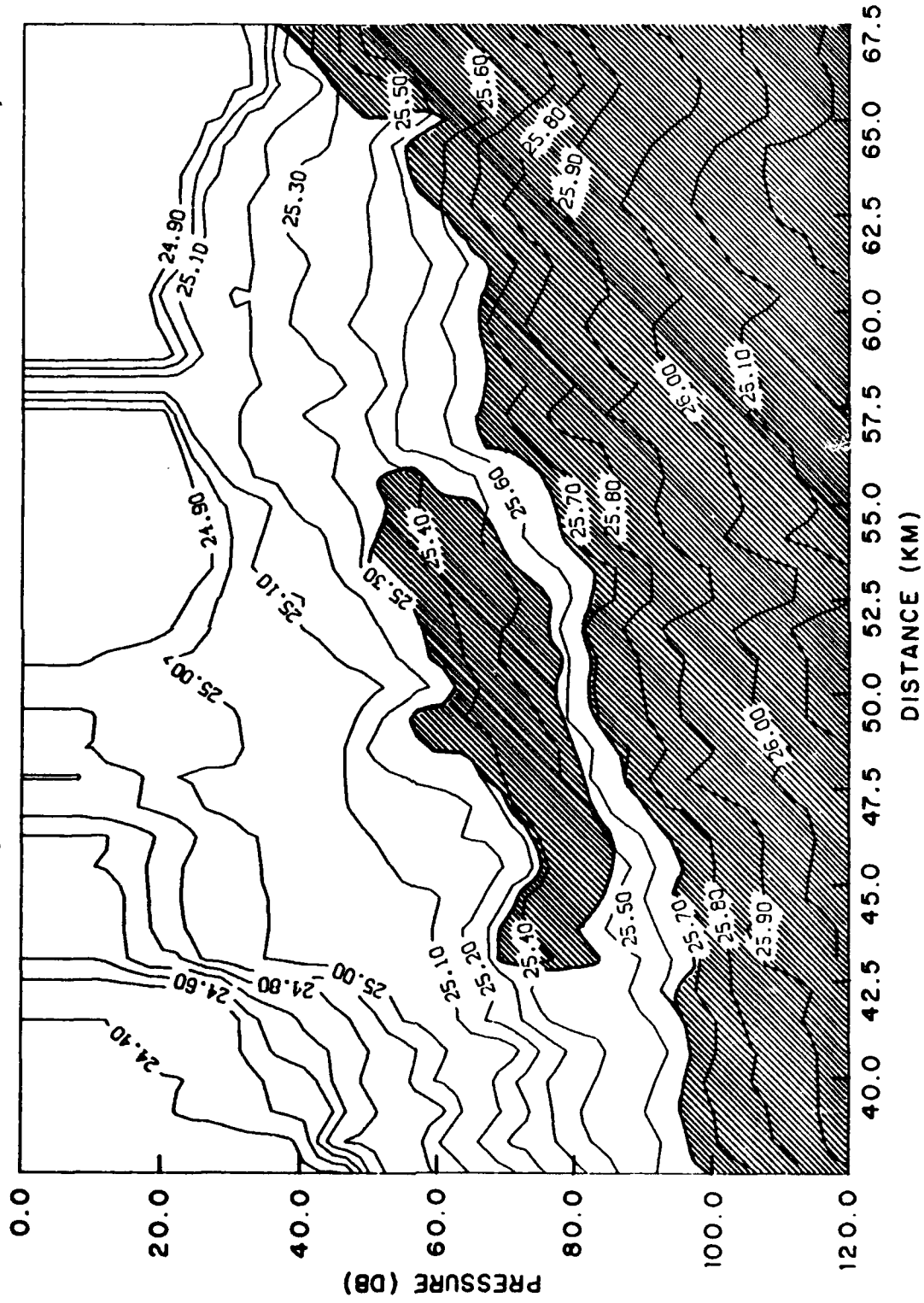


FIG. 4B

SALINITY (psu) OPT 21 TRANSECT 3

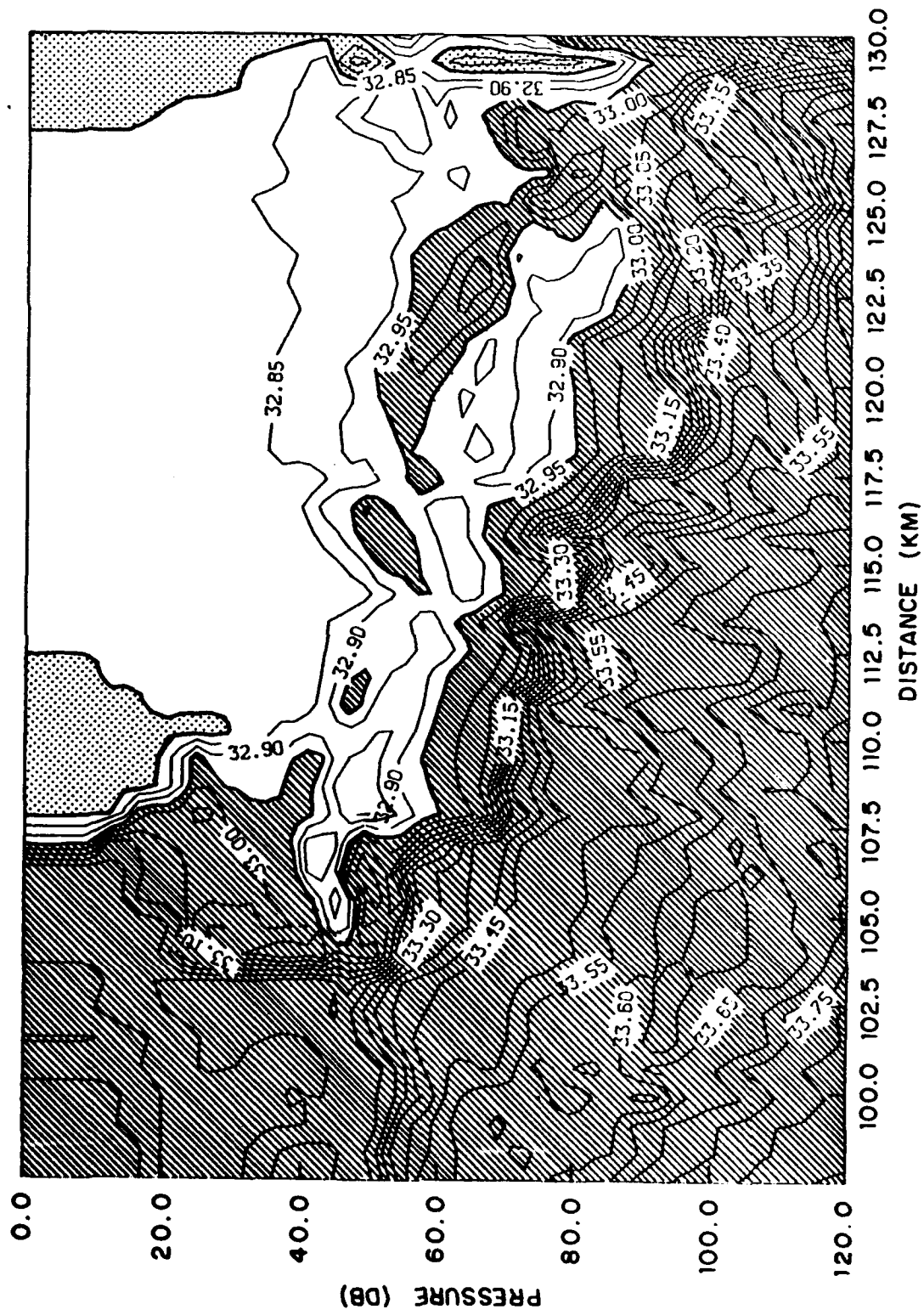


Fig. 5A

$\sigma_0$  (Kg/m<sup>3</sup>) OPT 21 TRANSECT 3

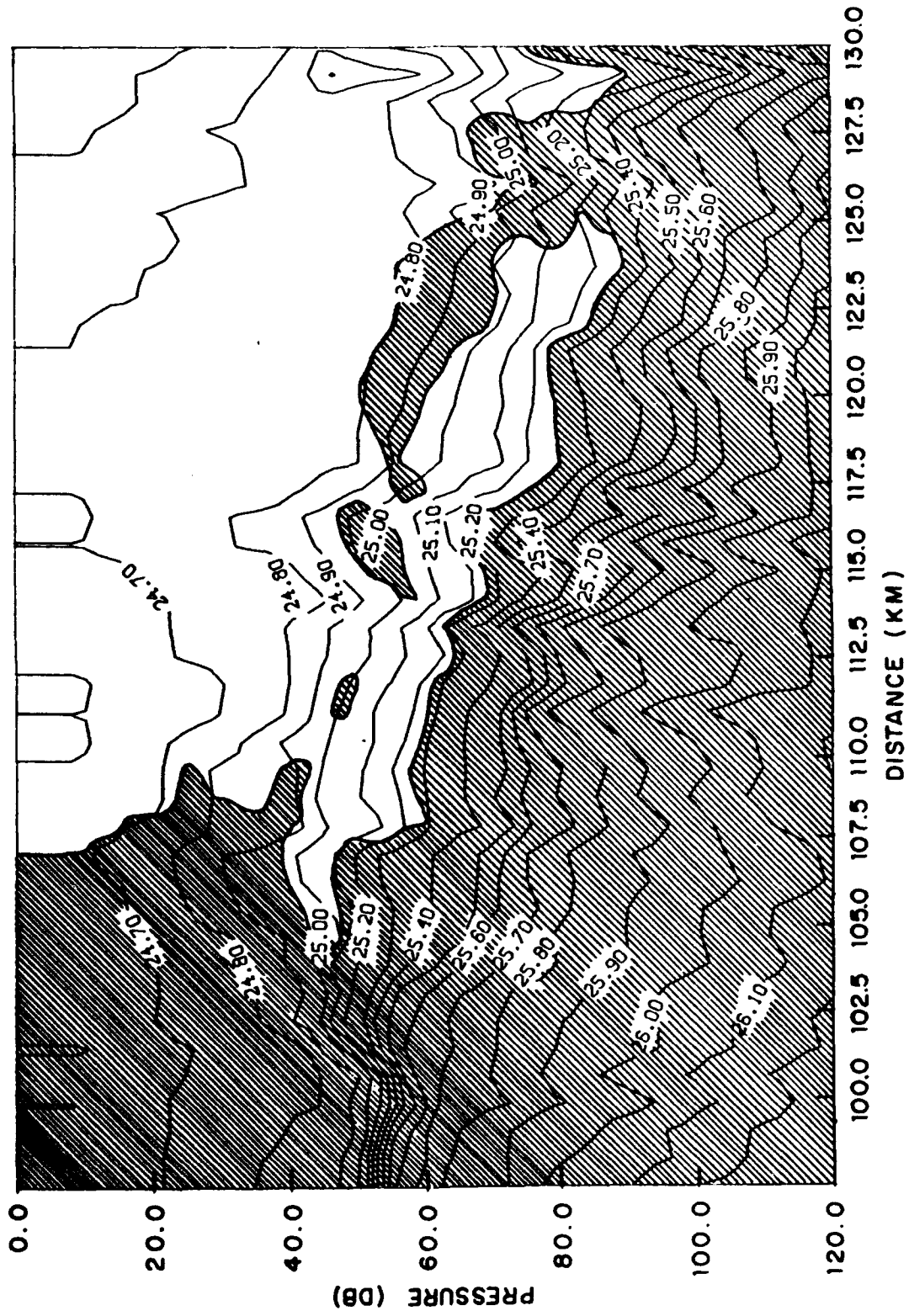


FIG. 5B

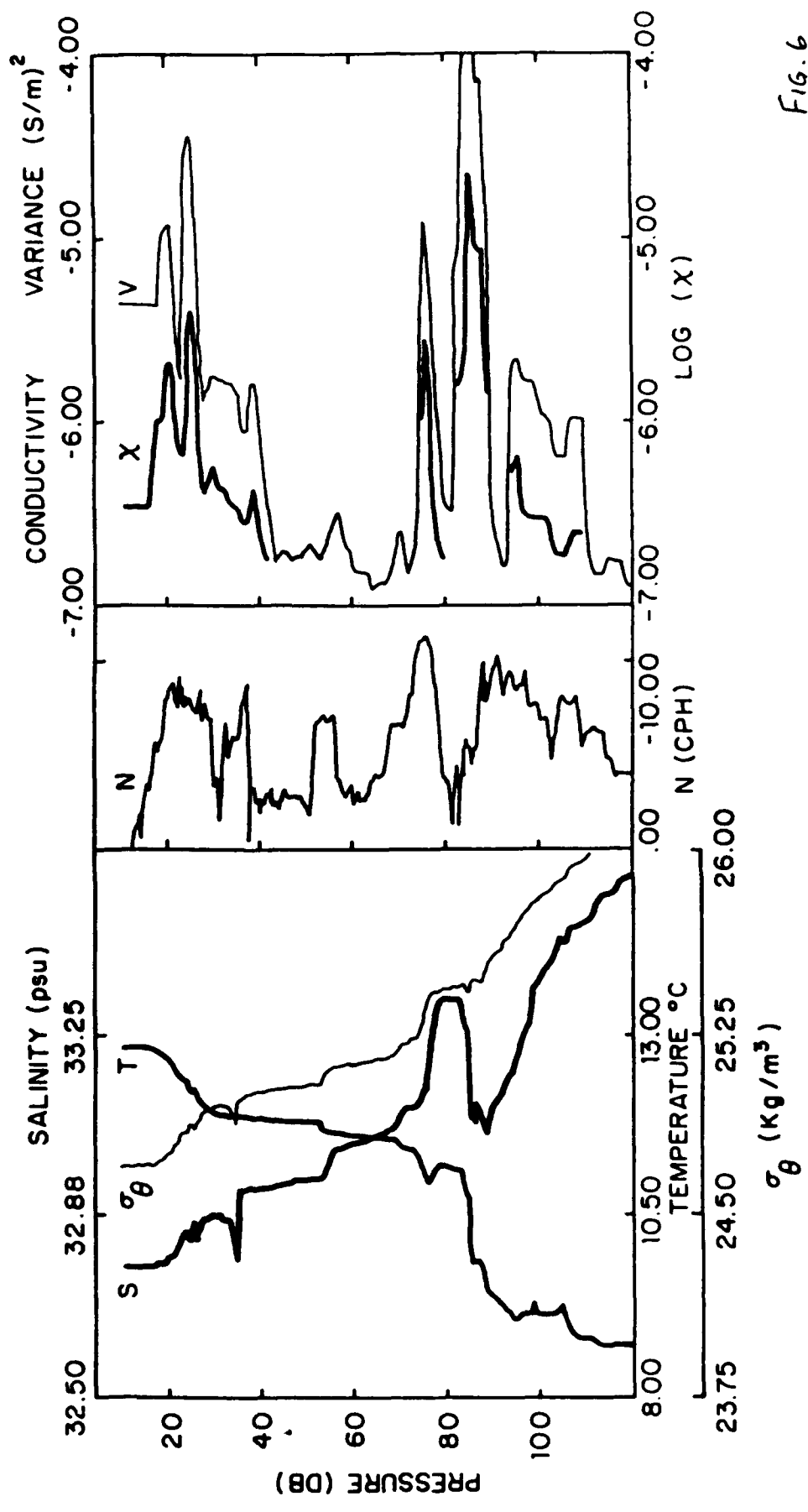


Fig. 6

